Nanotechnol. Environ. Eng. (2017) 2:6
https://doi.org/10.1007/s41204-017-0017-8

ORIGINAL PAPER

An artificial neural network (ANN)-based framework for the Cr removal from the spiked water samples by chitosan oligosaccharide-coated iron oxide nanoparticles

Sudeep Shukla[1,4] · Ujjwal Kumar[2] · Amit Prakash[3] · V. K. Jain[1]

Received: 6 February 2017 / Accepted: 17 April 2017 / Published online: 26 April 2017

Abstract Chromium contamination in water has become a major concern worldwide due to its adverse health effects. Chitosan oligosaccharide-coated iron oxide nanoparticles (CSO-INPs) were used in the present study for the magnetic separation of chromium from a chromium spiked water samples. Transmission electron microscope–energy-dispersive X-ray spectroscopy elemental mapping and scanning electron microscope–energy-dispersive X-ray spectroscopy elemental analysis were carried out to confirm the successful removal of the contaminant (total Cr) from the spiked water samples. A feedforward artificial neural network (ANN) model has been developed to predict the optimum efficiency of chromium ions removal from aqueous solution by CSO-INPs. Both the batch experiments and the ANN have been applied to assess the impact of various factors such as pH, nanoparticles dose, temperature, and time influencing the Cr removal efficiency of CSO-INPs. Removal efficiency has been found to be higher at low pH, with higher dose of nanoparticles at higher temperature. The ANN simulation further gives us a set of desired conditions (pH 3, CSO-INPs dose 0.7 mg/ml, temperature 28–30 °C, time 60 min) to achieve an optimum Cr removal efficiency of CSO-INPs.

✉ Ujjwal Kumar
ujjwalkumarin@yahoo.co.in

[1] School of Environmental Sciences, Jawaharlal Nehru University, New Delhi 110067, India

[2] School of Environment and Natural Resources, Doon University, Dehradun 248012, India

[3] Department of Environmental Science, Tezpur University, Tezpur 784028, India

[4] Amity School of Earth and Environmental Sciences, Amity University Haryana, Gurugram 122413, India

Graphical Abstract

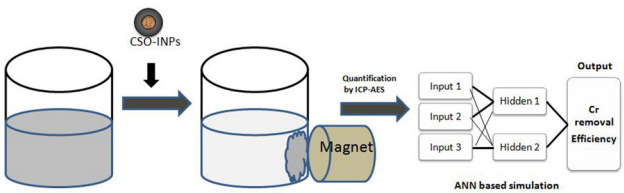

Keywords Chromium · Chitosan oligosaccharide · Iron nanoparticles · Artificial neural network (ANN)

Introduction

Chromium (Cr) is a hard, steel-grey metallic element that is listed by the United States Environmental Protection Agency (USEPA) as one of 129 priority pollutants [1]. The corrosion resistance properties of chromium made it highly useful in various industries, such as metal fabrication, metal finishing, plating, corrosion control, pigments and tanning compounds, and wood preservatives [2]. The effluents from these industries contribute a significant amount of chromium to soil, water bodies, and the ground water. Although Cr oxidation states range from (−II) to (+VI), however, only the Cr(+III) and Cr(+VI) states are stable in the natural environment [3]. Chromium (III), the most common form of chromium (Cr) in the natural environment, is not very soluble under normal groundwater conditions due to the formation of insoluble solid $Cr(OH)_3$ and Cr_2O_3 form.

Chromium (VI) exists in the natural environment as part of several compounds, and Cr(VI) is generally present in solution as monomeric forms: H_2CrO_4, $HCrO4^-$ (hydrogen

chromate), CrO_4^{2-}, and CrO_3 (chromium (III) oxide) or as $Cr_2O_7^{2-}$ (dichromate) [4]. The relative concentration of the various Cr(VI) species depends on the pH and the total Cr(VI) concentration within the normal pH range in natural waters (i.e. 6–8), and the CrO_4^{2-}, $HCrO4^-$ and $Cr_2O_7^{2-}$ ions are the forms expected [5]. Above a pH of about 6, CrO_4^{2-} generally dominates. Below pH of about 6, $HCrO^{4-}$ dominates when the Cr(VI) concentrations are relatively low, but $Cr_2O_7^{2-}$ becomes more significant as Cr(VI) concentrations increases. Due to its higher solubility, Cr(VI) can be transported to greater distance in groundwater.

Cr(III) is an essential nutrient, but exposure to its higher levels via inhalation, ingestion, or dermal contact may cause adverse health effects [6]. Cr(VI) is a carcinogen and a strong oxidizing agent. Exposure to higher doses of Cr(VI) possibly can induce mutations in living cells by damaging DNA–protein cross-linkages [7, 8]. Trace amounts of Cr^{+3} (50–200 µg/day) are essential for the maintenance of normal glucose metabolism in humans [9, 10]. The EPA standard for total Cr (as Cr^{6+}) in regulated drinking water in public water system is 0.1 mg/L (http://www.epa.gov/your-drinking-water/table-regulated-drinking-water-contaminants). The WHO recommends a limit of 0.05 mg/L total Cr (as Cr^{+6}) in drinking water [11], and the same has also been adopted by Bureau of Indian Standards [12].

Remediation technologies for bringing chromium concentrations below the regulatory limits primarily aim at reducing its oxidation state from Cr(IV) to Cr(III), and this also determines the type and cost of the treatment [13].

Chromium is dominantly removed by surface reduction of Cr(VI) to Cr(III) followed by adsorption of Cr(III) [14]. Recent advances in nanotechnology have suggested that nanoparticles can be explored for applications in water and wastewater treatment [15]. Nanomaterials (<100 nm), owing to their high specific surface area, short intraparticle diffusion distance, and tunable pore size and surface chemistry exhibit properties such as fast dissolution, high reactivity, and strong sorption. The surface of many nanomaterials can be functionalized to target specific contaminants, achieving high selectivity. Iron nanomaterials (INPs in their many oxidation states) have been widely utilized for the removal of heavy metals (Cr, Cu, Ni, Pb, Hgetc) from the various environmental matrices [13, 16–19]. The iron nanoparticles were also found to be effective for the detoxification of chlorinated compounds (chlorinated organic solvents, organochlorine pesticides, trinitrotoluenes, phenols, herbicide molinateetc [20, 21]. Surface modification of INPs with biopolymers such as chitosan not only increases the stability of the bare INPs in the aqueous environment [22–24], but also increases its adsorption potential against the heavy metal pollutants [25–27]. Application of chitosan as oligosaccharide may solve the solubility issue for environmental and biological applications. Due to its low molecular weight, chitosan oligosaccharide showed superior solubility in water and physiological solutions [28].

The nanomaterials-based chemical adsorption process is governed by several factors such as pH, temperature, concentration of pollutants, time of exposure, dose of nanomaterial, and others. Since there is large variation in adsorption efficiency (pollutant removal efficiency) with the variations in these factors, therefore, it is pertinent to optimize the combinations of different factors in a way so as to get the maximum removal efficiency. In order to achieve this objective, we need to set up a large number of experiments, which leads to a higher cost of the experimental procedures. However, a good model simulation of these processes can give insight into the dependence of removal efficiency on these factors and also gives us a set of conditions under which optimum removal efficiency can be achieved. Since using model simulation along with experiments provides more insight into the processes, this also helps us to reduce the number of experiments and hence reduction in cost of experiments as well [29–35]. Application of artificial neural network (ANN)-based model simulation has emerged as an effective tool for the same because of its well adaptability in linear/nonlinear simple/complex systems. Earlier published works corroborate the mileages of the ANN-based simulations for the optimization of adsorption of the heavy metal pollutants like Cr, Pb, Cu, and As [36–39]. Prakash et al. [28] have applied five-layer ANN neural network for the prediction of biosorption efficiency of the sawdust for the removal of copper(II) from the wastewater samples. They reported that the outcome of ANN-based model was found to be very close to the experimental values. Ranjan et al. [39] have compared two optimization techniques, response surface methodology (RSM) and artificial neural network (ANN) to evaluate the biosorptive remediation of arsenic (As) from batch samples. They have reported the outperformance of the ANN over the RSM for the prediction of the nonlinear behaviour of the system. Yetilmezsoy and Demirel [27] have utilized three-layer artificial neural network (ANN) model to predict the Pb ion removal efficiency of Antep pistachio (*Pistacia vera*) shells, from the aqueous solution. They report that the ANN model exhibited a good prediction of the experimental data.

In this study, experiments were conducted to estimate the removal efficiency of CSO-INPs for the removal of total Cr from the spiked water sample in simulated condition. For model simulation of the process, artificial neural network (ANN) has been used and applied to get a set of conditions that led to the optimum efficiency. To the best of our knowledge, the use of CSO-INPs along with ANN-

based optimization has been carried for the first time to remove total Cr from the aqueous system.

Materials and methods

Synthesis of CSO-INPs

CSO-INPs have been synthesized by chemical synthesis method as reported in our previous published study [24]. Iron oxide nanoparticles have been synthesized as reported by Jana et al. [40]. The oleic acid on the particle surface was replaced with a –COOH containing silane [41]. Nanoparticles were further functionalized with chitosan oligosaccharide via carbodiimide activation, using EDC and NHS [22].

Sample preparation

The Cr stock solution of 1000 mg/l concentration was prepared by dissolving 2.829 g $K_2Cr_2O_7$ (analytical reagent grade) in 1000 ml deionized–distilled water. Cr solution (working concentration) was prepared from suitable serial dilution of the stock solution. Total chromium in the control and treated sample was analysed by inductively coupled plasma–atomic emission spectrometry (ICP–AES, Horiba).

Removal of chromium in simulated conditions

After incubation, chitosan oligosaccharide-coated iron oxide nanoparticles (CSO-INPs) with chromium (20 mg/L) spiked water, a magnetic field by permanent magnet was applied to separate out the nanoparticles/heavy metal aggregates. SEM along with EDX studies of magnetically deflected nanoparticles/heavy metal aggregate was carried out to analyse the morphological and chemical characteristic of the aggregate. TEM images were recorded on a TEM, operated at an accelerating voltage of 20 kV. TEM equipped with an energy-dispersive X-ray analyser (EDX) (JEOL 2100F) was further used to characterize the elemental composition of CSO-INPs and the presence of metal pollutant (Cr ion) on the nanoparticles. Samples for TEM analysis were prepared by adding 10 µl of the nanoparticles-treated solution on 200-mesh carbon-coated Cu grids. The presence of chromium on the surface of CSO-INPs was further confirmed by the SEM equipped with energy-dispersive X-ray analyser (EDX; *Zeiss EVO40*).

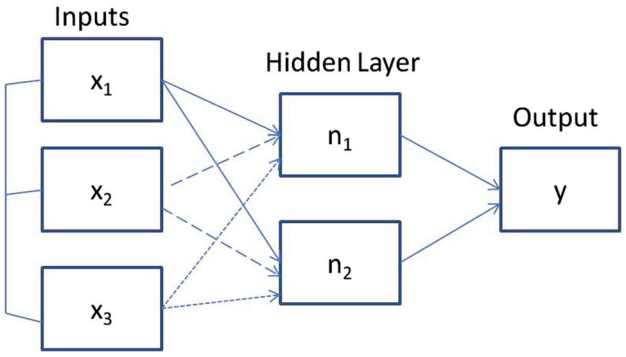

Fig. 1 Feedforward neural network

Batch experiments for the estimation of Cr removal efficiency of CSO-INPs

The 50 ml Cr solution of different concentration was treated with different concentrations (0.1, 0.3, 0.5 and 1 mg/ml) of CSO-INPs at different temperatures (28 and 38 °C), in constant temperature shaker (300 rpm). Samples were taken periodically from the mixture and subjected to an external magnetic field. Simulated studies were carried out at different pH, temperature, and the dose of nanoparticles. The solution pH was adjusted to the desired values including 2, 3, 5, 8, and 10 by using HCl and NaOH solution to evaluate the effect of pH on adsorption of Cr. The Cr removal efficiency of CSO-INPs has been calculated using the following formula.

$$\%\ \text{Metal Uptake} = \frac{(\boldsymbol{C}1 - \boldsymbol{C}2)}{\boldsymbol{C}1} \times 100$$

$C1$ = initial total chromium concentration (in solution) and $C2$ = final total chromium concentration (in solution).

Artificial neural network (ANN)-based modelling

Like the linear and polynomial approximation (regression) methods, a neural network relates a set of input variables $\{x_i\}$, $i = 1, 2,\ldots, k$, to a set of one or more output variables,$\{y_j\}$, $j = 1, 2,\ldots, k$. The difference between a neural network and the other regression methods is that the neural network makes use of one or more hidden layers, in which the input variables are squashed or transformed by a special function, known as a logistic or sigmoid/log-sigmoid transformation [42]. ANN explanation in this section and the following section has directly been adapted from McNelis [42].

Feedforward networks

Figure 1 illustrates the architecture on a neural network with one hidden layer containing two neurons, three input variables $\{x_i\}$, $i = 1, 2, 3,\ldots$, and one output y. We see *parallel processing*. In addition to the sequential processing of typical linear systems, in which only observed

inputs are used to predict an observed output by weighting the input neurons, the two neurons in the hidden layer process the inputs in a parallel fashion to improve the predictions. The connectors between the input variables, often called *input neurons*, and the neurons in the hidden layer, as well as the connectors between the hidden layer neurons and the output variable, or *output neuron*, are called synapses. The following equations describe this network

$$n_k = \omega_k + \sum_{i=0}^{i^*} \omega_k x_i$$

$$N_k = L(n_k) = \frac{1}{1 + e^{-n_k}}$$

$$y = \gamma_0 + \sum_{k=1}^{k^*} \gamma_k N_k$$

where $L(n_k)$ represents the log-sigmoid activation function. In this system, there are i^* variables $\{x\}$ and k^* neurons. A linear combination of these input variables $\{x_i\}$, $i = 1, 2,\ldots, i^*$, with the coefficient vector or set of input weights $\omega_{k,i}$, $i = 1, 2,\ldots, i^*$, as well as the constant term, $\omega_{k,0}$, forms the variable n_k. This variable is squashed by the logistic function and becomes a neuron N_k. The set of k^* neurons are combined in a linear way with the coefficient vector $\{\gamma_k\}, k = 1, 2, \ldots, k^*$ and taken with a constant term γ_0, to form the output y. The feedforward network coupled with the log-sigmoid activation functions is also known as the multilayer perceptron or MLP network. It is the basic workhorse of the neural network approach. In the present study, $i^* = 5$, in which, x_1, x_2, x_3, x_4, and x_5 are pH, temperature, dose of nanoparticles, initial pollutant concentration, and time, respectively. The number of neurons in the hidden layer has been taken as $n = 20$.

For finding the set of coefficients or weights $\Omega = \{\omega_{k,i}, \gamma_k\}$ in a network with a single hidden layer, we minimize the loss function Ψ, defined as the sum of squared differences between the actual observed output y and $\hat{y}$, and the output predicted by the network:

$$\min \Psi(\Omega) = \sum_{t=1}^{T} (y_t - \hat{y}_t)^2$$

$$\hat{y}_t = f(x_t; \Omega)$$

where T is the number of observations of the output vector y and $f(x_t; \Omega)$ is a representation of the neural network. Clearly, $\Psi(\Omega)$ is a nonlinear function of Ω. All nonlinear optimizations start with an initial gue of the solution, Ω_0, and search for better solutions, until finding the best possible solution within a reasonable amount of searching. In this study, Levenberg–Marquardt back propagation technique has been used for searching the solutions [43].

Result and discussion

Magnetic removal of CSO-INPs/Cr aggregate from the spiked water

The synthesized CSO-INPs were found to be homogeneously spherical in shape, having an average diameter of 9.1 ± 2.3 nm. CSO-INPs were found to be colloidally stable at various pH, making them suitable for environmental stable [23]. Figure 2a shows the deflected aggregate of CSO-INPs/Cr under the influence of an external magnetic field. TEM image of the deflected aggregates in Fig. 2b indicates that no morphological changes took place in CSO-INPs due to the adsorption of the chromium ion on the surface. Elemental mapping by TEM–EDX (JEOL 2100F) confirms the presence of Cr ion on the CSO-INPs

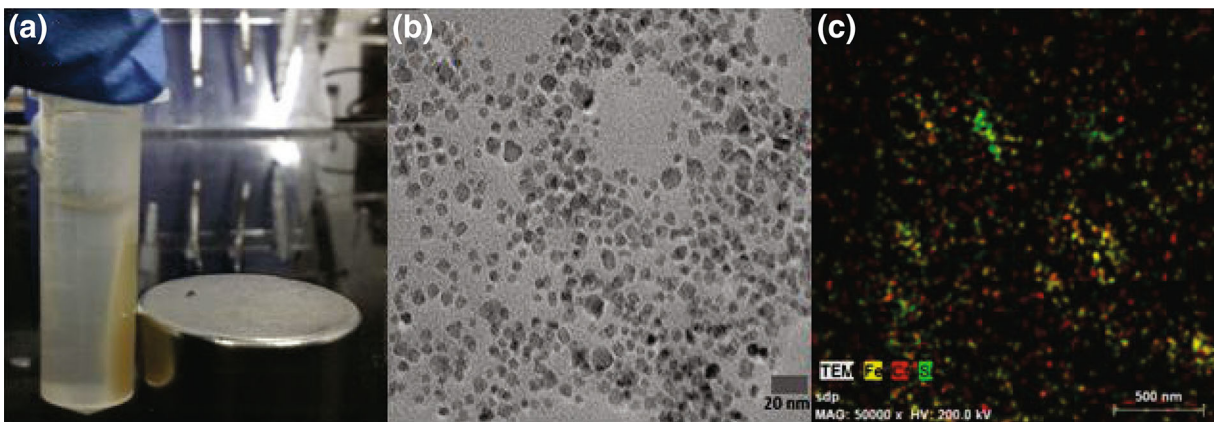

Fig. 2 **a** Nanoparticles–heavy metal aggregated mass deflected under magnetic field. **b** TEM image of deflected nanoparticles–heavy metal aggregate. **c** Elemental mapping of CSO-INPs/chromium aggregate

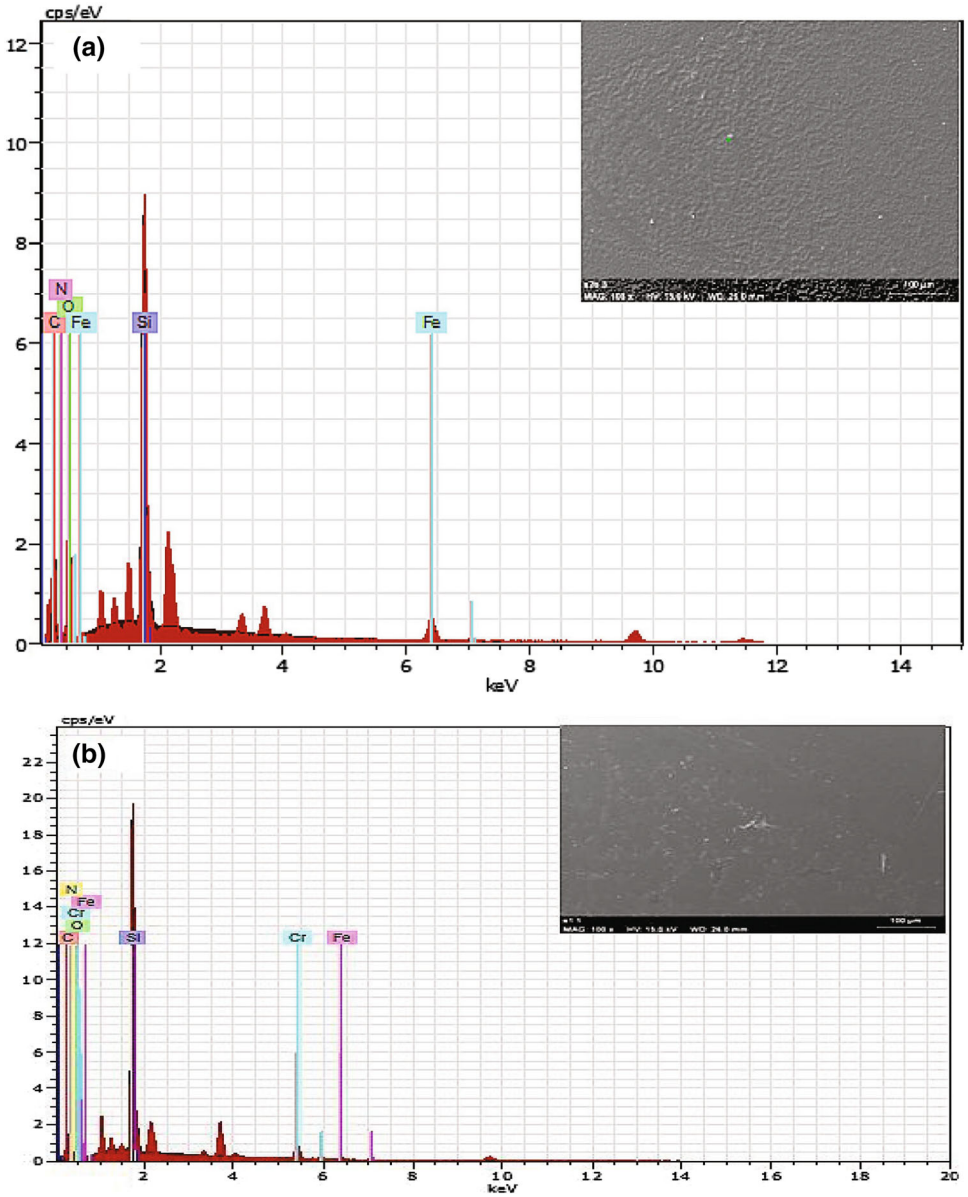

Fig. 3 **a** SEM–EDX elemental analysis of magnetically CSO-INPs aggregate (control). **b** SEM–EDX elemental analysis of CSO-INPs/chromium aggregate

aggregate (shown with red dots in Fig. 2c). The analysis of SEM–EDX (*Zeiss EVO40*; Fig. 3b) also confirms the presence of chromium on the deflected aggregate of CSO-INPs along with the spectral signatures of the constituent elements of CSO-INPs. SEM–EDX spectra of the control sample (untreated with chromium in Fig. 3a) show the presence of the constituent elements of the CSO-INPs having silane as a covalent linker (C, O, N, Si, and Fe).

Interaction of CSO-INPs with anionic chromium (exist CrO_4^{2-}, $HCrO4^-$, and $Cr_2O_7^2$ form at pH 6–8) could be attributed to the metal–nanoparticles complex formation through protonated $-NH_2$ and anionic metal through the process of chelation, adsorption, ion exchange/electrostatic attraction [44], by the formation of tertiary complex [45] and adsorption

ANN modelling and validation

In ANN modelling, 60% of the experimental data have been used for building up the ANN model, 20% data have been kept for validation purpose, and rest 20% data have been used purely for testing. Figure 4 shows the comparison between experimental and model simulated values. Figure 4a–c clearly indicates a strong correlation ($\sim$0.99) between experimental and model simulated values of Cr removal efficiency for the training, validation as well as the test data cases. The subsequent sections discuss the effect of various factors (pH, dose, temperature, initial pollutant concentration, and time) on Cr removal efficiency based on both the ANN model simulations and experimental results.

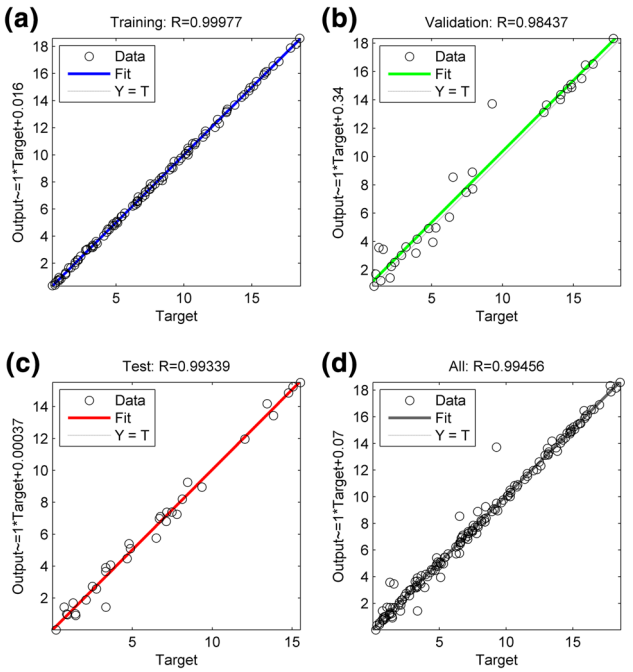

Fig. 4 ANN validation: from *top left*, *top right* to *bottom left* and *bottom right* **a** training: experimental versus simulated output, **b** validation experimental versus validation output, **c** testing: experimental versus testing output, **d** all: experimental versus model output

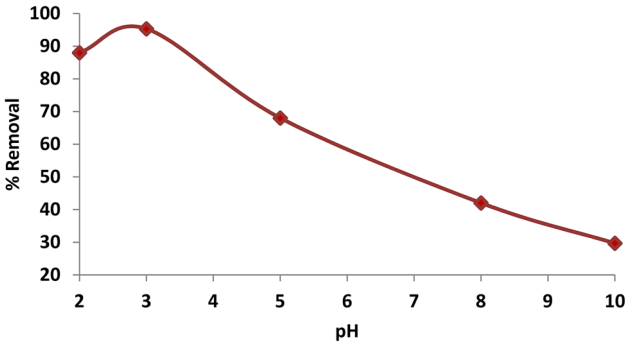

Fig. 5 Percentage Cr removal efficiency of CSO-INP at various pH (2, 3, 5, 8, 10) of chromium spiked water sample at temperature 28 °C, nanoparticles dose 0.5 mg/ml, initial pollutant conc 20 ppm, and time 60 min

Batch experiments and ANN Model to evaluate Cr removal efficiency of CSO-INPs

The batch experiments were performed to evaluate the Cr removal efficiency of CSO-INPs at different pH (2, 3, 5, 8, 10), for different doses of CSO-INPs (0.1, 0.3, 0.5, 0.9, 1.0 mg/ml) at different temperatures (28, 38 °C) and for different initial pollutant (Cr) concentrations (10, 20 ppm). Once the ANN model has been prepared and validated as discussed in "ANN modelling and validation" section, the ANN simulation has been carried out to obtain the Cr removal efficiency for varying inputs pH (2, 3, 4, 5, 6, 7, 8, 9, 10), CSO-INPs doses (0.1, 0.2, 0.3, 0.4, 0.5, 0.6, 0.7, 0.8, 0.9, 1 mg/ml), initial pollutant concentrations (10, 15, 20, 25, 30, 35 ppm), temperatures (20, 25, 28, 30, 35, 38, 40, 45 °C). The following sections discuss the effect of pH, CSO-INPs doses, and temperature on Cr removal efficiency of CSO-INPs on the basis of both the batch experiments and the ANN simulation.

Effect of pH on percentage removal of total Cr

The effect of pH on the Cr removal efficiency has been examined at various pH (2, 3, 5, 8, 10). Figure 5 shows the experimental results of variation in percentage Cr removal efficiency with different pH at 28 °C temperature, nanoparticles dose of 0.5 mg/ml for initial Cr concentration of 20 ppm after time 60 min. To get more insight into the results, the ANN simulated values of Cr removal efficiency are shown in Fig. 6.

Both the results clearly indicate that the pH plays an important role to determine the Cr removal efficiency. Figures 5 and 6 clearly show that, in general, with increase in pH, Cr removal efficiency decreases. However, removal efficiency at pH 3 was observed greater than at pH 2 (Fig. 5). ANN-based model simulation (Fig. 6) shows high efficiency at pH 2 and 3; notably, at pH 3, higher efficiency could be achieved at lower dose (0.6–0.7 mg/ml). Here, ANN-based model outcomes provide additional insight about the multifactor dependence of the CSO-INPs removal potential. pH of solution not only determines the surface charge of the nanoparticles, but also the oxidation state of heavy metal pollutant. This may be attributed to deprotonation of the amino group of chitosan coating on iron oxide nanoparticles. Below the pKa value of chitosan, the sorbent is positively charged, while the chromium anions in solutions are negatively charged. This leads to an electrostatic attraction between the two. Above the pKa, the chitosan will be less protonated or neutral, and hence, Cr removal is reduced at pH higher than the pKa. Results corroborate maximum capture efficiency at pH 3, as below this pH, Cr exists in solution in the form of H_2CrO_4 the strong competition for adsorption sites between H_2CrO_4 and protons [27].

Effect of nanoparticles dose on Cr removal efficiency

Varying dose of CSO-INPs (0.1, 0.3, 0.5, and 1 mg/ml) was treated for different time interval (10, 20, 30, 40, 50, 60 min) at different pH (2, 3, 5, 8, 10) and temperature (28, 38 °C), to illustrate the effect of CSO-INPs doses on the adsorption of Cr ions from the aqueous solution. ANN simulation has been done for CSO-INPs doses (0.1, 0.2, 0.3, 0.4, 0.5, 0.6, 0.7, 0.8, 0.9, 1 mg/ml) at different pH (2, 3, 4, 5, 6, 7, 8, 9, 10) and different initial Cr concentration

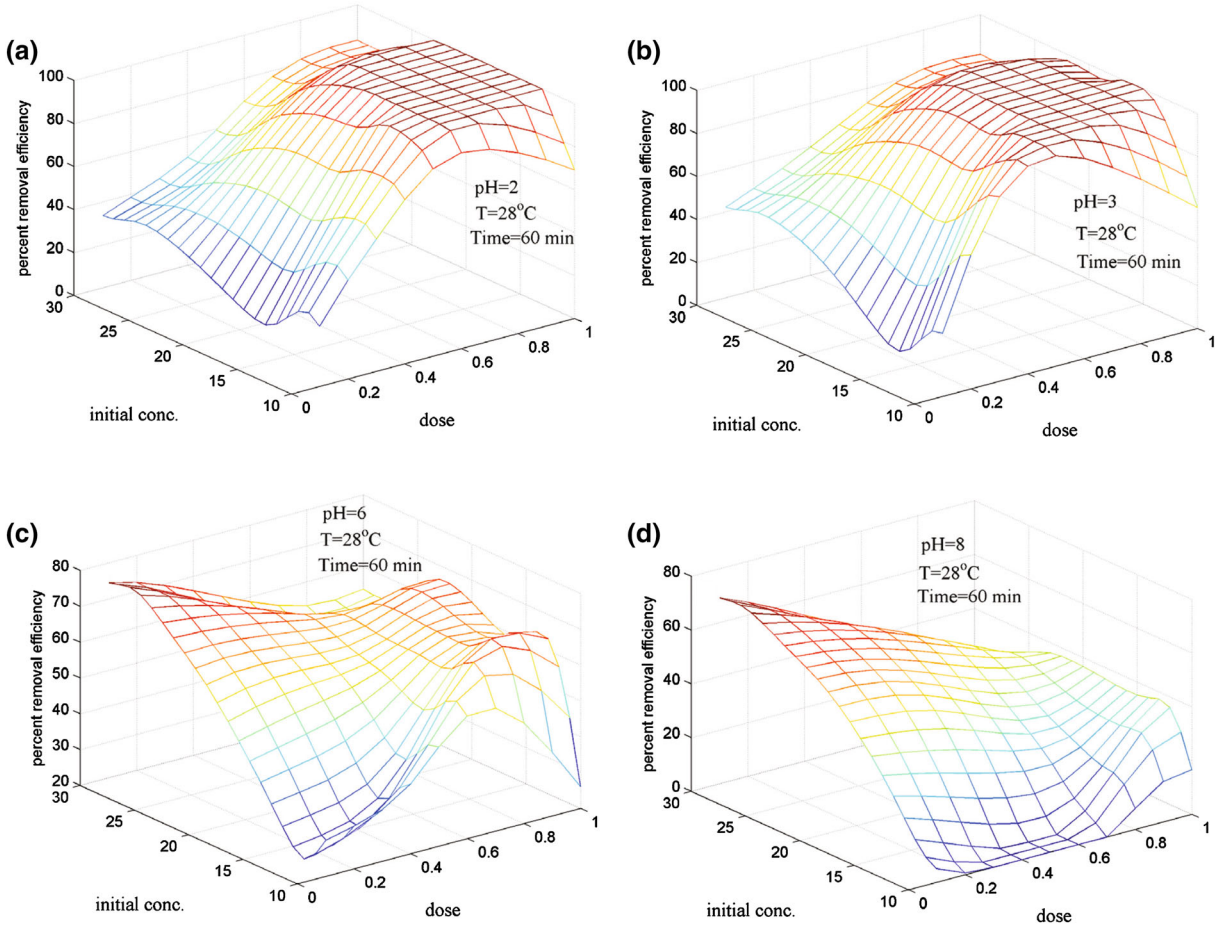

Fig. 6 ANN simulation: Cr removal efficiency versus initial Cr concentration and nanoparticles dose at **a** pH 2, **b** pH 3, **c** pH 6, and **d** pH 8

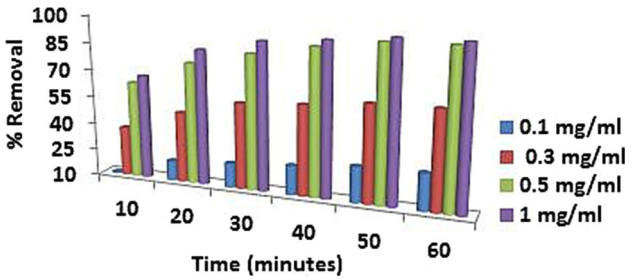

Fig. 7 Percentage Cr removal efficiency for different doses of CSO-INPs (0., 1, 0.3, 0.5, 1 mg/ml) at temperature 28 °C and pH 3

(10, 15, 20, 25, 30, 35 ppm). Figure 7 shows the experimental results of the dose-dependent Cr removal efficiency at different CSO-INPs doses while Fig. 8 shows the ANN simulated results of removal efficiency for different CSO-INPs doses at temperature 28 °C after time 60 min.

Cr removal efficiency of CSO-INPs was found to be increased with the increase in the concentration of adsorbent (CSO-INPs) dosage in Figs. 7 and 8. This may be attributed to the increase in overall surface area of the adsorbent (CSO-INPs) which, in turn, increases the number of pollutant (Cr) binding sites. However, Fig. 7 also reveals that after a fixed time there is no significant increase in capture efficiency, which may be due to saturation of all binding sites with the pollutant.

ANN model output shows a correlation trend with the experimental values. Higher removal efficiency of CSO-INPs could be observed at higher doses (0.9, 1 mg/ml) of nanoparticles. However, for an economically efficient remediation process, a minimum dose of adsorbent with higher removal efficiency is desirable. ANN-based output clearly indicates that the higher removal efficiency could be obtained at low-dose condition (0.5 mg/ml) assisted by low pH condition (2 and 3) and moderate temperature (25–30 °C; Figs. 6, 8).

Effect of effective temperature on percentage adsorption efficiency

Experiments were carried out to evaluate the impact of different temperature conditions on the Cr removal efficiency of CSO-INPs. The batch experiments were conducted at 28 and 38 °C for the different doses of CSO-INPs

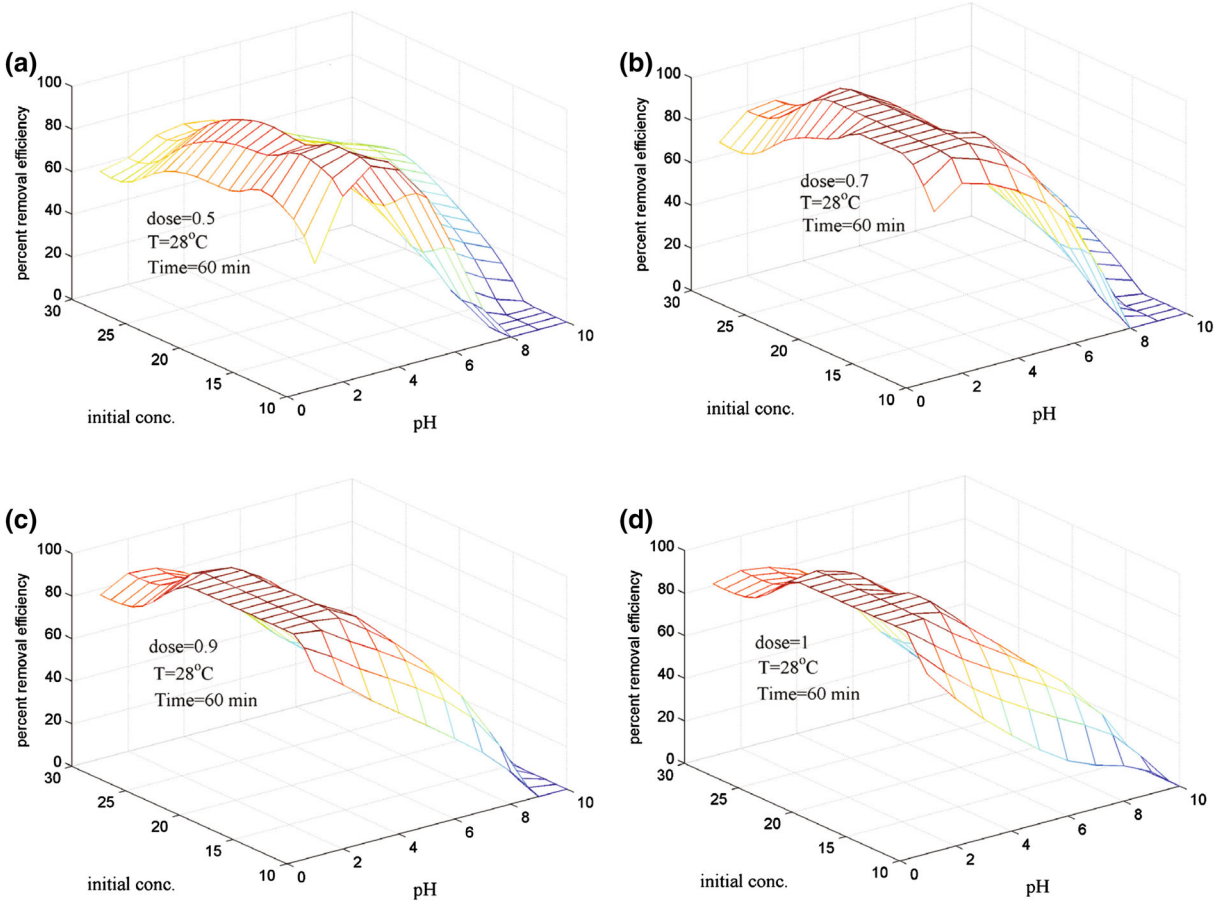

Fig. 8 ANN simulation: effect of CSO-INPs dose on Cr removal efficiency at different initial Cr concentration (10, 15, 20, 25, 30 ppm) and different pH conditions **a** pH 2, **b** pH 3, **c** pH 6, and **d** pH 8

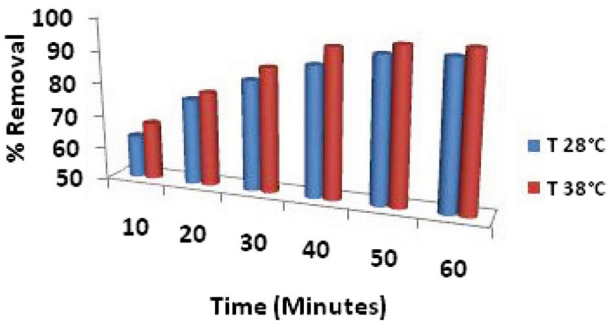

Fig. 9 Percentage Cr removal efficiency of CSO-INP at different temperature (28 and 38 °C) of the sample

(0.1, 0.3 0.5, and 1 mg/ml) and different pH (2, 3, 5, 8, 10) conditions for different time interval (10, 20, 30, 40, 50, 60 min). ANN simulation has been carried out to obtain the Cr removal efficiency for different temperatures conditions (20, 25, 28, 30, 35, 38, 40, 45 °C) at varying inputs pH (2, 3, 4, 5, 6, 7, 8, 9, 10), CSO-INPs doses (0.1, 0.2, 0.3, 0.4, 0.5, 0.6, 0.7, 0.8, 0.9, 1 mg/ml), initial pollutant concentrations (10, 15, 20, 25, 30, 35 ppm). Figure 9 indicates that an increase in temperature induces higher Cr removal efficiency. Figure 10a–d shows the ANN simulation of Cr removal efficiency for a wider range of temperatures (25, 28, 30, 38 °C). The ANN model outcome also shows the similar trend. The increase in Cr removal efficiency with an increase in temperature may be attributed to an increase in colliding frequency between Cr with the CSO-INPs at higher temperature [25] that ultimately results into an increase in the value of rate constant leading to the higher adsorption at active sites of CSO-INPs.

Effect of time of contact on percentage Cr removal efficiency

The results in Figs. 7 and 9 indicate that the Cr removal efficiency varies with time at a given pH, temperature, CSO-INPs dose, and initial Cr concentration. It can be seen that the rate of Cr uptake was initially quite slow, followed by high removal rate then gradually attaining an equilibrium condition. Major amount of the Cr gets removed during the first 50 min of the reaction attaining a saturation by 60 min. It may be hypothesized that by 60 min, all active sites of CSO-INPs get occupied by the heavy metals.

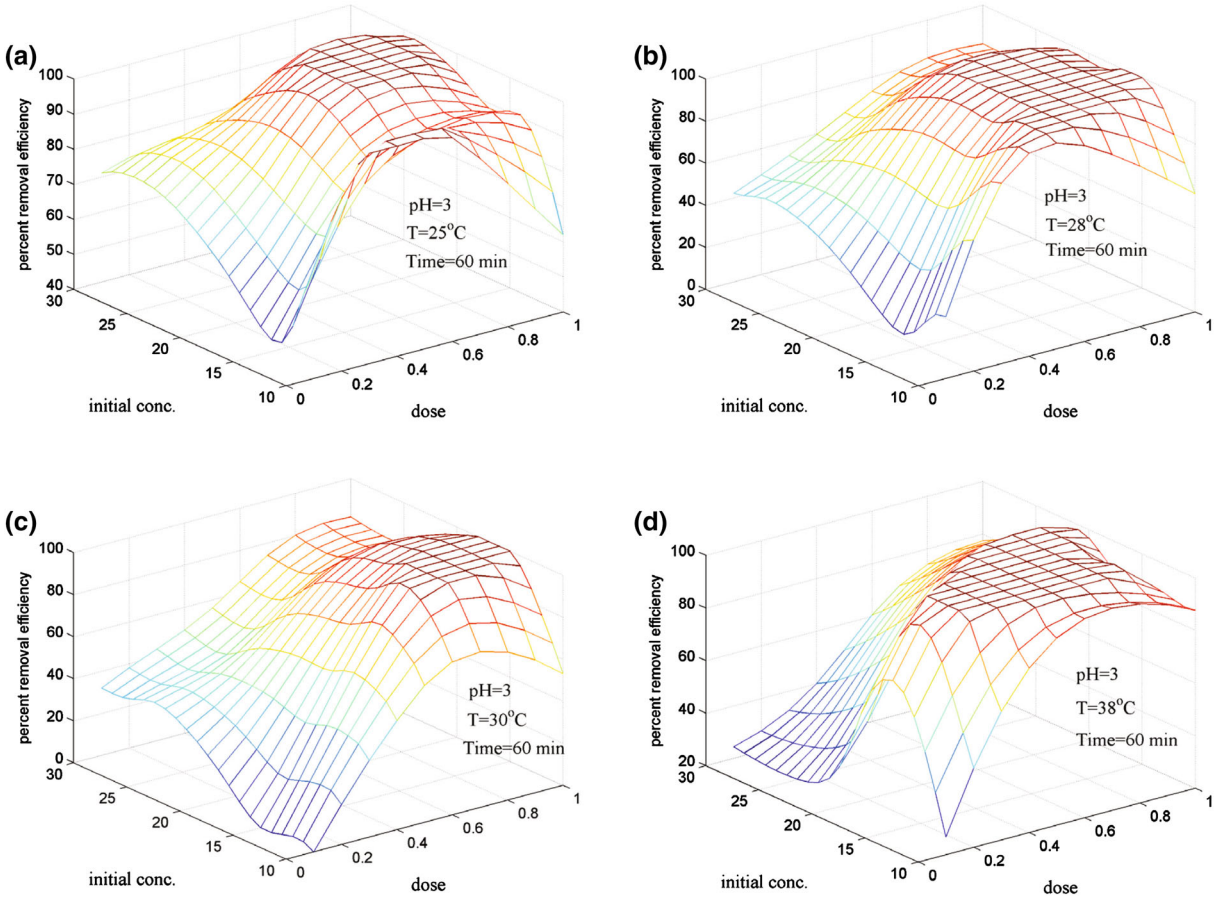

Fig. 10 ANN simulation: effect of CSO-INPs dose on Cr removal efficiency at different temperature conditions **a** 25 °C, **b** 28 °C, **c** 30 °C, and **d** 38 °C

Conclusion

The results of batch experiments reveal the potential application of CSO-INPs for the magnetic removal of the Cr from the contaminated aqueous system. The batch experiments and the ANN simulation explain the effect of various factors (pH, temperature, CSO-INPs dose, and time) on the Cr removal efficiency of CSO-INPs. The higher Cr removal efficiency has been observed at low pH, higher dose of CSO-INPs. The ANN simulation further gives us a set of desired conditions (pH 3, CSO-INPs dose = 0.7 mg/ml, temperature = 28–30 °C, time = 60 - min) to achieve an optimum Cr removal efficiency of CSO-INPs. The present study suggests that the CSO-INPs can be successfully used for the treatment of the Cr-contaminated aqueous system. Further research should be carried out to investigate the sorption of Cr in the presence of other component of natural system for the application of CSO-INPs for the removal of heavy metals in different environmental matrices.

Acknowledgements Sudeep Shukla, one of the authors of the present study, was recipient of fellowship from Council of Scientific and Industrial Research (CSIR), India. We are thankful to School of Environmental Sciences, Jawaharlal Nehru University and Advanced Instrumentation Research Facility (AIRF), JNU, New Delhi for their financial and technical support.

References

1. Morrison Robert D, Murphy Brian L (2006) Environmental forensics: contaminant specific guide. Academic Press, San Diego
2. Bielicka A, Bojanowska I, Wiśniewski A (2005) Two faces of chromium—pollutant and bioelement. Pol J Environ Stud 14:5–10
3. Malaviya P, Singh A (2011) Physicochemical technologies for remediation of chromium-containing waters and wastewaters. Crit Rev Environ Sci Technol 41:1111–1172. doi:10.1080/10643380903392817
4. Palmer CD, Wittbrodt PR (1991) Processes affecting the remediation of chromium—contaminated Sites. Environ Health Perspect 92:25–40
5. Hawley EL, Deeb RA, Kavanaugh MC, Jacobs JA (2004) Treatment technologies for chromium (VI). In: Guertin J, Jacobs JA, Avakian CP (eds) Chromium handbook. CRC Press, Boca Raton, pp 273–308
6. Zhitkovich A (2011) Chromium in drinking water: sources, metabolism, and cancer risks. Chem Res Toxicol 24:1617–1629. doi:10.1021/tx200251t

7. Dayan AD, Paine AJ (2001) Mechanisms of chromium toxicity, carcinogenicity and allergenicity: review of the literature from 1985 to 2000. Hum Exp Toxicol 20:439–451. doi:10.1191/096032701682693062
8. Stearns DM, Kennedy LJ, Courtney KD et al (1995) Reduction of chromium (VI) by ascorbate leads to chromium-DNA binding and DNA strand breaks in vitro. Biochemistry 34:910–919
9. Anderson RA, Cheng N, Bryden NA et al (1997) Elevated intakes of supplemental chromium improve glucose and insulin variables in individuals with type 2 diabetes. Diabetes. doi:10.2337/diabetes.46.11.1786
10. Anderson RA (1997) Chromium as an essential nutrient for humans. Regul Toxicol Pharmacol 26:S35–S41. doi:10.1006/rtph.1997.1136
11. Gorchev HG, Ozolins G (2011) WHO guidelines for drinking-water quality. WHO Chron 38:104–108. doi:10.1016/S1462-0758(00)00006-6
12. Bureau of Indian Standards (2012) IS 10500 (2012): Indian Standard Drinking water—Specification (Second Revision), ICS 13.060.20
13. Owlad M, Aroua MK, Daud WAW, Baroutian S (2009) Removal of hexavalent chromium-contaminated water and wastewater: a reaview. Water Air Soil Pollut 200:59–77. doi:10.1007/s11270-008-9893-7
14. Huang L, Cheng X, Liu C et al (2009) Preparation, characterization, and antibacterial activity of oleic acid-grafted chitosan oligosaccharide nanoparticles. Front Biol China 4:321–327. doi:10.1007/s11515-009-0027-4
15. Qu X, Alvarez PJJ, Li Q (2013) Applications of nanotechnology in water and wastewater treatment. Water Res 47:3931–3946. doi:10.1016/j.watres.2012.09.058
16. Hu J, Chen G, Lo IMC, Asce M (2004) Selective removal of heavy metals from industrial wastewater using maghemite nanoparticle: performance and mechanisms. J Environ Eng 132:709–715. doi:10.1061/(ASCE)0733-9372(2006)132:7(709)
17. Kumpiene J, Ore S, Renella G et al (2006) Assessment of zerovalent iron for stabilization of chromium, copper, and arsenic in soil. Environ Pollut 144:62–69. doi:10.1016/j.envpol.2006.01.010
18. Jabeen H, Chandra V, Jung S et al (2011) Enhanced Cr(VI) removal using iron nanoparticle decorated graphene. Nanoscale 3:3583–3585. doi:10.1039/c1nr10549c
19. Ngwenya CZ, Ntwampe KSO, Silwana N (2016) Synthesis of metallic nanoparticles from Beta vulgaris using a single-pot green chemistry approach and their environmental engineering application. Nanotechnol Environ Eng 1:11. doi:10.1007/s41204-016-0012-5
20. Xu P, Zeng GM, Huang DL et al (2012) Use of iron oxide nanomaterials in wastewater treatment: a review. Sci Total Environ 424:1–10. doi:10.1016/j.scitotenv.2012.02.023
21. Ali I (2012) New generation adsorbents for water treatment. Chem Rev 112:5073–5091. doi:10.1021/cr300133d
22. López-Cruz A, Barrera C, Calero-DdelC VL, Rinaldi C (2009) Water dispersible iron oxide nanoparticles coated with covalently linked chitosan. J Mater Chem 19:6870–6876. doi:10.1039/b908777j
23. Rinaudo M (2006) Chitin and chitosan: properties and applications. Prog Polym Sci 31:603–632. doi:10.1016/j.progpolymsci.2006.06.001
24. Shukla S, Jadaun A, Arora V, Kumar R (2015) In vitro toxicity assessment of chitosan oligosaccharide coated iron oxide nanoparticles. Toxicol Rep 2:27–39. doi:10.1016/j.toxrep.2014.11.002
25. Geng B, Jin Z, Li T, Qi X (2009) Kinetics of hexavalent chromium removal from water by chitosan-FeO nanoparticles. Chemosphere 75:825–830. doi:10.1016/j.chemosphere.2009.01.009
26. Boddu VM, Abburi K, Talbott JL, Smith ED (2003) Removal of hexavalent chromium from wastewater using a new composite chitosan biosorbent. Environ Sci Technol 37:4449–4456
27. Thinh NN, Hanh PTB, Ha LTT et al (2013) Magnetic chitosan nanoparticles for removal of Cr(VI) from aqueous solution. Mater Sci Eng C Mater Biol Appl 33:1214–1218. doi:10.1016/j.msec.2012.12.013
28. Son S, Chae SY, Choi C et al (2004) Preparation of a hydrophobized chitosan oligosaccharide for application as an efficient gene carrier. Macromol Res 12:573–580. doi:10.1007/BF03218446
29. AL-Othman ZA, Ali R, Naushad M (2012) Hexavalent chromium removal from aqueous medium by activated carbon prepared from peanut shell: adsorption kinetics, equilibrium and thermodynamic studies. Chem Eng J 184:238–247. doi:10.1016/j.cej.2012.01.048
30. Sharma G, Naushad M, Al-Muhtaseb AH et al (2017) Fabrication and characterization of chitosan-crosslinked-poly(alginic acid) nanohydrogel for adsorptive removal of Cr(VI) metal ion from aqueous medium. Int J Biol Macromol 95:484–493. doi:10.1016/j.ijbiomac.2016.11.072
31. Albadarin AB, Collins MN, Naushad M et al (2017) Activated lignin-chitosan extruded blends for efficient adsorption of methylene blue. Chem Eng J 307:264–272. doi:10.1016/j.cej.2016.08.089
32. Pandian AMK, Karthikeyan C, Rajasimman M (2017) Isotherm and kinetic studies on adsorption of malachite green using chemically synthesized silver nanoparticles. Nanotechnol Environ Eng. doi:10.1007/s41204-016-0013-4
33. Alqadami AA, Naushad M, Abdalla MA, Khan MR, Alothman ZA (2016) Adsorptive removal of toxic dye using Fe_3O_4–TSC nanocomposite: equilibrium, kinetic, and thermodynamic studies. J Chem Eng Data. doi:10.1021/acs.jced.6b00446
34. Alqadami AA, Naushad M, Abdalla MA et al (2016) Synthesis and characterization of Fe_3O_4@TSC nanocomposite: highly efficient removal of toxic metal ions from aqueous medium. RSC Adv 6:22679–22689. doi:10.1039/C5RA27525C
35. Naushad Mu, Vasudevan S, Sharma G, Kumar A, ALOthma ZA (2016) Adsorption kinetics, isotherms, and thermodynamic studies for Hg^{2+} adsorption from aqueous medium using alizarin red-S-loaded amberlite IRA-400 resin. Desalin Water Treat 57:18551–18559
36. Yetilmezsoy K, Demirel S (2008) Artificial neural network (ANN) approach for modeling of Pb(II) adsorption from aqueous solution by Antep pistachio (*Pistacia vera* L.) shells. J Hazard Mater 153:1288–1300. doi:10.1016/j.jhazmat.2007.09.092
37. Prakash N, Manikandan SA, Govindarajan L, Vijayagopal V (2008) Prediction of biosorption efficiency for the removal of copper(II) by neural network.pdf. J Hazard Mater 158:1268–1275
38. Singh TN, Singh VK, Sinha S (2006) Prediction of cadmium removal using an artificial neural network and a neuro-fuzzy technique training of the network. Mine Water Environ 25:214–219
39. Ranjan D, Mishra D, Hasan SH (2011) Bioadsorption of arsenic: an artificial neural networks and response surface methodological approach. Ind Eng Chem Res 50:9852–9863
40. Jana NR, Chen Y, Peng X (2004) Size- and shape-controlled magnetic (Cr, Mn, Fe Co, Ni) oxide nanocrystals via a simple and general approach. Chem Mater 16:3931–3935
41. De Palma R, Peeters S, Van Bael MJ et al (2007) Silane ligand exchange to make hydrophobic super paramagnetic nanoparticles water-dispersible. Chem Mater. doi:10.1021/cm0628000
42. McNelis PD (2005) Neural networks in finance: gaining predictive edge in the market, 1st edn. Elsevier Academic Press, Boca Raton

43. Press WH, Teukolsky SA, Vetterling WT, Flannery BP (2007) Numerical recipes: the art of scientific computing, 3rd edn. Cambridge University Press, Cambridge
44. Guibal E (2004) Interactions of metal ions with chitosan-based sorbents: a review. Sep Purif Technol 38:43–74. doi:10.1016/j.seppur.2003.10.004
45. Piron E, Domard A (1998) Interactions between chitosan and α emitters: 238Pu and 241Am. Int J Biol Macromol 23:121–125. doi:10.1016/S0141-8130(98)00042-7